ACS OMEGA

http://pubs.acs.org/journal/acsodf

Article

Exploring SPK98 for the Selective Sensitization of ATM- or P53-Deficient Cancer Cells

Bhanu Priya, Gurudutt Dubey, and Sivapriya Kirubakaran*

Cite This: *ACS Omega* 2023, 8, 4954−4962

Read Online

ACCESS | Metrics & More | Article Recommendations | Supporting Information

ABSTRACT: Frequent mutation in the ATM/P53 signaling pathway has been documented in many human cancers. Reportedly, cancer cells with deficient P53/ATM pathways depend on functional Ataxia-telangiectasia and Rad3-related (ATR) protein for survival. This has prompted research in developing ATR inhibitors for the selective sensitization of cancer cells that are P53/ATM-deficient, but no clinical success has been attained thus far. This study explores the therapeutic potential of SPK98, an analogue of Torin2 in P53- and ATM-deficient cancer cells. Furthermore, the prospect of improving the therapeutic outcome of the genotoxic agent was also explored. SPK98 was shown to inhibit full-length human ATR protein purified from HEK293T cells. Cellular investigation using SPK98 demonstrated that it selectively sensitizes P53- and ATM-deficient cells at low concentrations compared to P53-/ATM-proficient cells. Furthermore, SPK98 drives the cancer cells toward cell death by promoting the formation of DNA double-strand breaks. Taken together, our findings suggest that SPK98 is a promising therapeutic molecule for P53- or ATM-deficient malignancy that merits additional preclinical investigation.

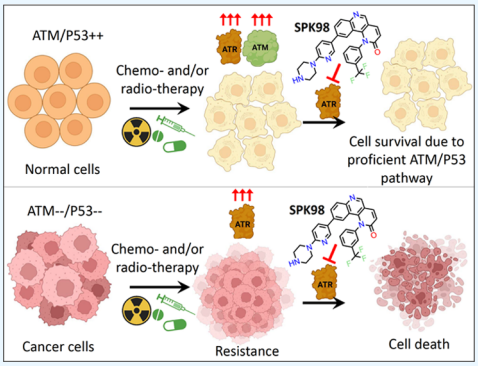

INTRODUCTION

The integrity of our genome is constantly threatened by a variety of chemicals and cellular processes that alter the DNA sequence/structure directly or indirectly.[1−3] DNA damage response (DDR) pathways are one of the fundamental cellular processes that maintain genome integrity through cellular pathways involved in but not limited to cell cycle checkpoints and DNA repair.[4] The DDR is organized into a variety of distinct yet functionally interrelated pathways that are primarily classified by the kind of DNA damage a cell encounters. Most DDR pathways include a similar set of highly orchestrated processes: DNA damage detection, activation of DDR regulators at the damage site, cell cycle arrest, and, ultimately, DNA repair or apoptosis.[5,6]

Ataxia-telangiectasia and Rad3-related (ATR) kinase is one of the apical kinases in the DDR pathway. It gets activated in response to single-stranded DNA (ssDNA) generated due to replication stress or DNA damage.[7] The ssDNA coated with RPA forms a nucleoprotein structure that acts as a backbone for the recruitment and activation of ATR-ATRIP via several other regulator proteins, including but not limited to Rad9−Rad1−Hus1 complex, Rad17complex, and TopBP1.[8−10] This protein complex helps in the activation of ATR. ATR phosphorylates and activates its effector kinase Chk1; once activated, it brings about functional change.[11] Increased expression of DDR proteins like ATR in many cancer types also limits the effectiveness of the genotoxic agent. Due to proficient DNA repair mechanisms, cancer cells overturn the induced damage resulting in chemo and radio-resistance.[12,13]

On the contrary, DDR pathway aberrations also predispose cells to cancerous growth. Aberrations of the DDR pathway are widely reported in different cancer types that not only allow the cells to grow uncontrollably but also make them overly dependent on other collateral pathways for survival.[14] A classic example is the dependence of HR (Homologous Recombination) repair-deficient (BRCA1−/− or BRCA2−/−) cancer cells on poly(ADP-ribose) polymerase (PARP)-mediated DNA repair.[15,16] Synthetically lethal strategies, in which cooperating pathways that DDR-defective cells rely on for survival are harnessed for therapeutic targeting, are becoming increasingly popular as a potential strategy to kill cancer cells with DDR aberrations (Figure 1). Thus, identifying other widespread DDR alterations can serve as predictive biomarkers and be exploited for their dependency on the other proteins.

The next-generation sequencing of a colorectal cancer patient's tumor sample has shown that ATM and P53 are two of the frequently altered gene. Colorectal tumors have a 60% prevalence of P53 gene alteration, which can be caused by deletion, mutation, or gene loss.[17−19] Abrogated functions of one of the P53 alleles frequently have a dominant negative

Received: November 16, 2022
Accepted: January 16, 2023
Published: January 30, 2023

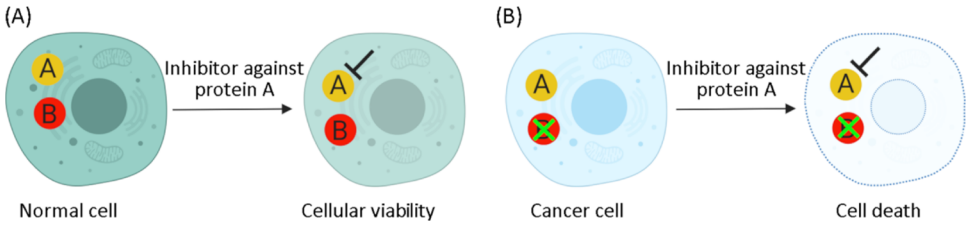

Figure 1. General representation of synthetic lethal interactions as a cancer therapeutic strategy. The loss of either gene A or B is conducive to cellular viability, while the loss of both genes altogether results in cellular death. (A) A normal cell with no mutation would be able to withstand gene A inhibition. (B) The abnormalities present in cancer cells (here in gene B) make them prone to cell death by inhibiting the counter protein (here protein A).

impact and inhibit wild-type P53 functions.[20] A significant fraction of patients with faulty P53 often have mutations in genes involved in p53 regulation, such as ATM, that result in compromised functioning of P53. ATM and P53 mutations are frequently linked with a poor prognosis and chemo-resistance, which has a negative clinical effect.[21−26] Previous studies have demonstrated that cancer cells having alterations in ATM/P53 pathway can get sensitized to ATR inhibition.[13,27−29] Also, unplanned DNA replication caused by oncogene activation leads to replication stress in frequently dividing cancer cells. Fork stalling and formation of ssDNA resulting from replication stress make the cells heavily dependent on functional ATR protein for survival.[30,31] All of these results suggest a therapeutic window due to tumor cells' excessive reliance on the ATR pathway as a result of oncogene-induced replication stress and/or compromised ATM-p53 pathway. This provides the scope for the rational design of small-molecule ATR inhibitors and explores their therapeutic potential in cancer therapeutics.

Currently, VX-970 M1774, AZD6738, RP-3500, and ART0380 are a list of a few ATR inhibitors that are in clinical trials.[32−36] Most of these studies are designed to check the efficacy of the aforementioned inhibitors for patients with ATM- or p53-deficient pathways or to overcome resistance to the genotoxic agent. Following the same lead, we previously synthesized and characterized SPK98, a Torin2 analogue, as a potential ATR/mTOR inhibitor.[37,38] Torin2 is a potent inhibitor of the pan-PIKK kinase family.[39] However, genotype-specific studies exploring synthetically lethal approaches have not been investigated. Therefore, in this study, we have explored the therapeutic potential of SPK98 in ATM- or p53-deficient/mutated cells. Also, the potential of SPK98 was tested to overcome radiation resistance.

MATERIALS AND METHODS

Plasmid, Cell Lines, and Cell Culture. Plasmid pcDNA3-ATR WT (Plasmid #31611) and pLV.ATMi (Plasmid #14542) were procured from addgene, and pcDNA3.1(+) was a kind gift from Dr. Sharmistha Majumdar (IIT Gandhinagar). HEK293T, HCT116, and HCT116-ATM_KD cells were cultured in Dulbecco's modified Eagle medium (DMEM) with 10% fetal bovine serum (FBS) and incubated at 37 °C with 5% CO_2. HEK293T and HCT116 were procured from the National Centre for Cell Sciences (NCCS), Pune, India.

Transfection. For the expression optimization of the full-length ATR for purification, pcDNA3-ATR WT and pcDNA3.1(+) backbone was transfected using Lipofectamine 3000 into HEK293T cells. Forty-eight hours post-transfection, the cells were irradiated with 50 mJ of UV-C and cells were lysed 1 h post-irradiation. For the generation of ATM knockdown HCT116 cell lines, pLV.ATMi shRNA plasmid was transfected in HCT116 using Lipofectamine 3000. Three days post-transfection, the ATM knockdown cells were selected by growing them in antibiotic selection media (complete DMEM + 1 μg/mL of puromycin). Later, the cells were maintained in a stringent selection condition of 4 μg/mL puromycin.

Immunoprecipitation of the ATR WT from HEK293T. HEK293T cells were seeded in a 150 mm cell culture dish. Six to eight hours post-seeding, the cells were transfected with 35 μg of pcDNA3-Flag-ATR using lipofectamine 3000. At the time of transfection, the confluency of the cells should not be more than 70%. Forty-eight hours post-transfection, the cells were irradiated with 50 mJ of UV. One hour post UV treatment, the cells were washed with phosphate-buffered saline (PBS) and lysed in radioimmunoprecipitation assay buffer (RIPA) buffer (R0278-50ML) containing protease phosphatase inhibitor. The lysate was sonicated to enrich the DNA-bound ATR. The soluble fractions of the lysate were incubated with 100 ul of EZview Red ANTI-FLAG M2 Affinity Gel at 4 °C with rocking for 4 h. The bead-bound protein was collected by centrifugation at 10,000 rpm for 5 min. The beads were washed with TBS three times, with decreasing concentration of NaCl (From 1 M to 150 μM). Finally, the protein was eluted in TBS containing 200 μg/mL 3× Flag peptide.

Western Blotting. The cells were seeded in a 60 mm dish. After transfection and incubation, the cells were lysed in RIPA buffer with protease and phosphatase inhibitors. The soluble fraction of the lysate was loaded on the sodium dodecyl sulfate (SDS) gel (6% for ATM and 12% for apoptosis marker), and the protein was transferred to a poly(vinylidene fluoride) (PVDF) membrane (0.45 μm for ATM and 0.22 μm for apoptosis marker). The PVDF membrane was blocked with 5% nonfat dried milk in TBST for 1.5 h and then incubated with primary antibody at 4 °C for 14 h with shaking. The membrane was further incubated with a secondary antibody for 2 h after washing the membrane with TBST. The blot was visualized using enhanced chemiluminescence (ECL) substrate. For apoptotic marker analysis, HCT116-ATM_KD cells were treated with 10 nM SPK98 for 24 h.

In Vitro Kinase Assays. The biological activity of the full-length ATR protein was evaluated, and enzyme inhibition was carried out using the ADP-Glo Kinase Assay (Promega, Madison, WI). The kinase reaction was performed on a solid white 96-well plate with a 20 μL reaction setup containing 620 ng ATR kinase, 10 μM P53 peptide, 100 μM ATP, and kinase buffer (40 mM Tris-Cl (pH 7.5), 20 mM $MgCl_2$, and 0.1 mg/mL bovine serum albumin). The assay also contained

https://doi.org/10.1021/acsomega.2c07356
ACS Omega 2023, 8, 4954−4962

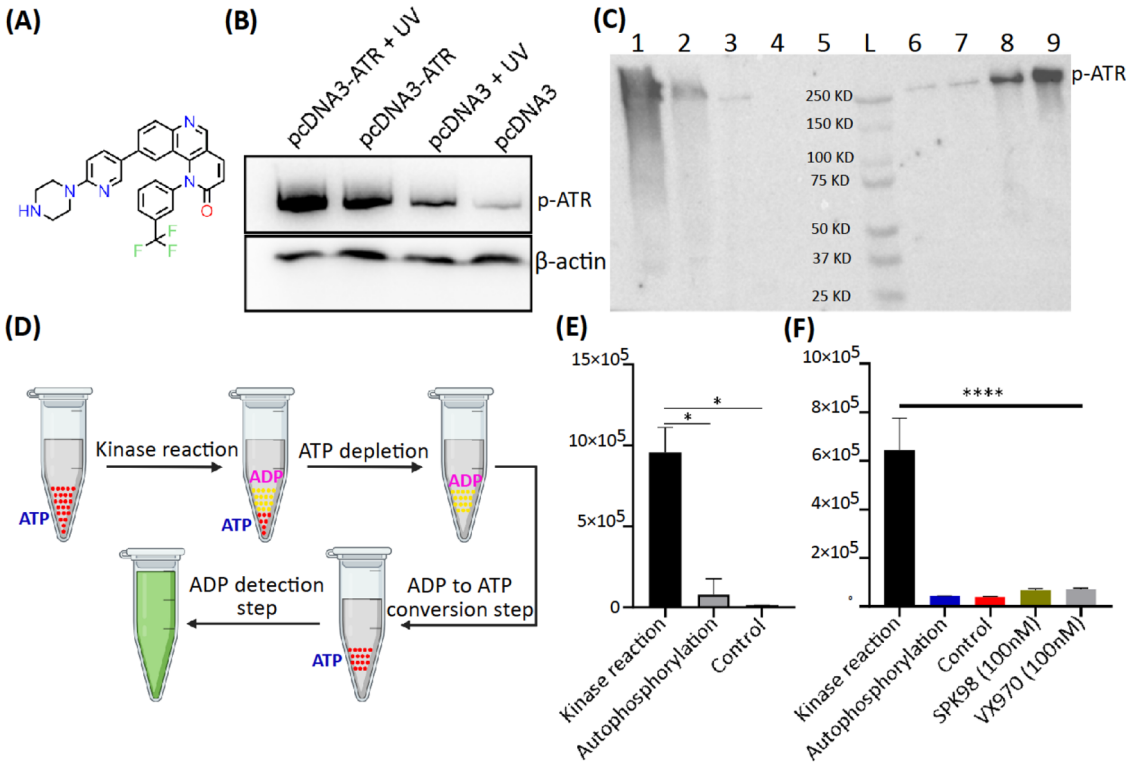

Figure 2. (A) Structure of SPK98. (B) Expression of p-ATR under different transfection conditions. (C) Flag affinity pulldown of FLAG-ATR. Full-length active ATR obtained from the FLAG affinity purification; Lane 1: whole cell lysate, Lane 2: unbound fraction, Lanes 3−5: wash fractions with wash buffer Tris-Cl at pH 7.4 containing 1 M NaCl (Lane 3) and 150 mM NaCl (Lanes 4, 5); Lanes 6−9: p-ATR in the elution fractions. (D) Workflow of the in vitro kinase assay. (E) Purified ATR was subjected to kinase reactions to check its phosphorylation activity. Statistical analysis was done by a two-tailed unpaired Student *t*-test ($*P < 0.05$, $n = 3$). (F) Kinase assay in the presence of SPK98 and VX-970. One-way analysis of variance (ANOVA) comparison was performed to compare the kinase activity ($P < 0.0001$, $n = 3$).

appropriate controls lacking protein, substrate, and ATP. By adding ATP, reactions in each well were initiated and maintained at 37 °C for an hour. The kinase reaction was then terminated, and the unused ATP was depleted by adding 20 μL of the ATP depletion reagent to each well for 40 min. Finally, the ADP generated from the kinases reaction was converted to ATP by adding 40 μL of kinase detection solution to each well and incubated for 1 h. ATP was then measured through luminescence using an EnVision multilabel plate reader (PerkinElmer, Inc., MA). The luminescence intensity correlates to the kinase activity.

Cell Viability Analysis. Around 2000 cells are seeded in each well of the white 96-well tissue culture plate. The cells are treated with SPK98 for 72 h; following this, Cell Titer-Glo reagent is added. After 10 min of incubation in the dark, a luminescence reading was taken using an EnVision multilabel plate reader (PerkinElmer, Inc., MA).

Clonogenic Assay. For combinatorial treatment of UV and SPK98, around 1×10^5 cells were seeded in a 20 mm dish. After 48 h of 10 nM SK98 treatment, the cells were exposed to 50 mJ of UV radiation and then maintained in old media containing SPK98 for an additional 24 h. The cells were allowed to grow for 3−4 weeks to form colonies. Colonies were fixed with 100% methanol and stained using 0.2% crystal violet. Colonies growing in a group of 50 cells or more were counted in a stereomicroscope. For SPK98 monotherapy, 1×10^5 cells were seeded in a 20 mm dish. The cells were treated with 10 nM SK98 for 72 h, following which around 1000 cells were seeded in a 20 mm plate. The cells were allowed to grow for 14 days to form colonies.

Immunocytochemistry. 5×10^5 HCT116-ATM_KD cells were seeded on poly L-lysine-coated coverslips. The cells were incubated in a humidified CO_2 incubator at 37 °C for 12 h after receiving a 10 nM SPK98 treatment. The culture media for the relevant treatment group was then saved prior to the 50 mJ UV-C exposure treatment and added back after irradiation. The cells were rinsed with PBS and fixed with 4% paraformaldehyde for 15 min after 3 h of incubation. The cells were permeabilized using 100% methanol solution for 10 min. Blocking with 3% fetal bovine serum in TBST for 1 h was carried out. The cells were incubated with γH2AX antibody at 4 °C for 14 h. Following this, the cells were incubated with Alexa Fluor 488 conjugate anti-rabbit secondary antibody for 2 h at room temperature. The cells were mounted using Antifade Mounting Medium containing DAPI. Confocal laser scanning microscopy was used to visualize γH2AX foci.

Protein Structure Modeling. Protein structures of the ATR, ATM, and DNA-PK kinase domain were modeled using the SWISS-MODEL server on the template proteins with PDB IDs 4JSP, 7NI5, and 7K0Y, respectively. The modeled structures were minimized using molecular mechanics force field and validated using ERRAT plot, Verify 3D, Ramachandran plot, and PROCHECK.

Molecular Docking. Protein crystal structures of mTOR (PDB 4JSV), PI3K-γ (PDB 5G55), PI4KB (5FBL), and PIK3C3 (3LS8) were obtained from the Protein Data Bank. The crystal structures and models of proteins were subjected to protein preparation steps, including adding hydrogens, removing water molecules, optimization of H atoms, and further minimization. SiteMap analysis was performed for

https://doi.org/10.1021/acsomega.2c07356
ACS Omega 2023, 8, 4954−4962

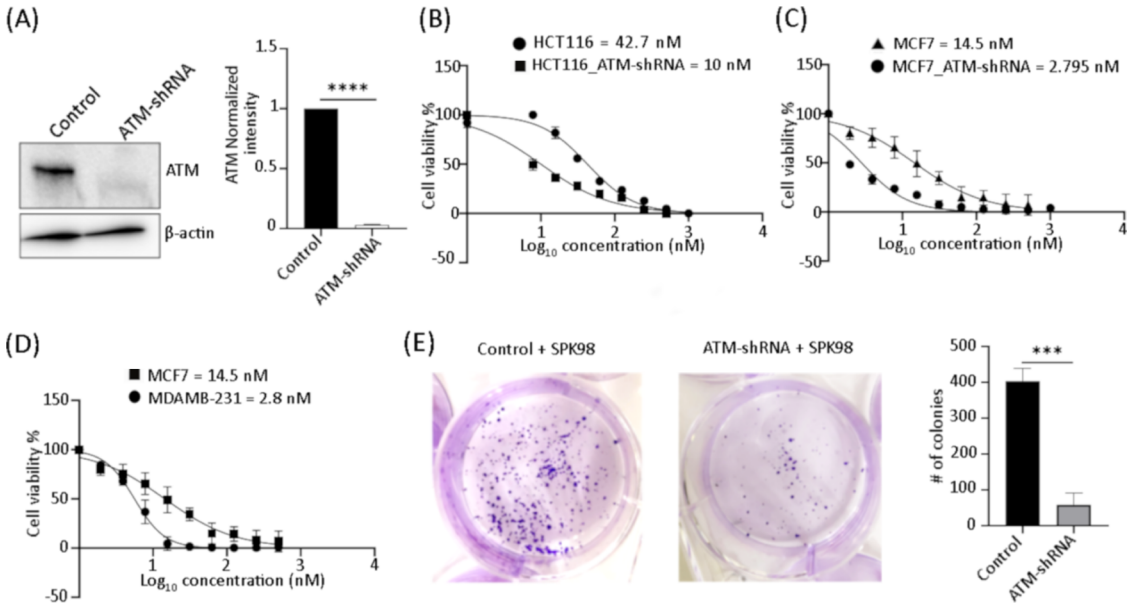

Figure 3. (A) Western blot analysis of ATM level in HCT116 and ATM knockdown HCT116 cells and densitometry quantification. Two-tailed unpaired Student *t*-test was performed to compare band intensity (****$P < 0.0001$, $n = 3$). Cell viability curves of ATM-deficient or -proficient (B) HCT116 and (C) MCF7 and cells with different (D) P53 profiles treated with SPK98. (E) Clonogenic assay of SPK98-treated HCT116-ATM_KD cells. Representative images of single-cell clone proliferation, stained with crystal violet, and colony numbers were compared using two-tailed unpaired Student *t*-test (***$P < 0.001$, $n = 3$).

ATM, ATR, mTOR, and DNA-PK to recognize the cavity for the docking analysis. The best druggable site for docking was identified in each protein's catalytic domain (near the hinge region). Receptor grids were generated on the centroid of the ligands in PI3K-γ, PI4KB, and PIK3C3, and grid validation was done by redocking the cocrystallized ligand of the respective proteins. Receptor grids on remaining proteins were generated on the centroid of the sitemap in the catalytic domain. The structure of SPK98 was drawn using 2D Sketcher, which was subjected to the ligand preparation without any constraints, considering all possible tautomers, ionic states, and stereoisomers to obtain all possible forms of its energy-minimized structures. Molecular docking of the prepared SPK98 molecule was performed using the Glide module of the Schrodinger software package at extra precision docking mode,[40] wherein the ligand was kept flexible, and the protein site was rigid. The XP score was considered as the docking score, and the binding pose of each protein−ligand complex was analyzed in XP Visualizer. Additionally, ADME analysis for SPK98 was also performed using the QikProp module.

MM-GBSA Binding Energy Calculation. The molecular mechanics with generalized Born and surface area solvation (MM-GBSA)[41] binding energy of all of the protein−ligand complexes were obtained using the Prime module of the Schrodinger software package. XP docked complexes were subjected to estimate binding free energy in kcal/mol unit. Prime MM-GBSA binding energy estimation takes the absolute energies of complex, ligand, and protein into account. The components of binding energy are coulomb energy, covalent binding energy, van der Waals energy, solvation energy, lipophilic energy, H-bond interaction energy, etc. The following equation was used in the prime binding energy calculation

$$\text{MM} - \text{GBSA}\ \Delta G_{\text{Bind}} = G_{\text{complex}} - [G_{\text{protein}} + G_{\text{ligand}}]$$

Software. All of the statistical analysis was carried out using GraphPad Prism. Confocal results were analyzed and quantified using Fiji: ImageJ image processing package. Using GIMP software, image panels were created. Molecular docking and image generation were done in Schrödinger Release 2022-3: Maestro, Schrödinger, LLC, New York, NY, 2021.

RESULTS

SPK98 Inhibits Full-Length ATR. To perform ATR enzyme inhibition studies with SPK98 (Figure 2A), the FLAG-ATR was expressed and purified from HEK293T cells. Since ATR requires multiple PTMs and protein partners to achieve its optimal kinase activity,[42] the cells were exposed to UV-C before proceeding with purification. UV-C treatment has been reported to significantly enhance the level of active ATR in cells.[43,44] This knowledge was used to increase the yield of active protein during purification. Cell lysates were immunoprecipitated using ANTI-FLAG M2 Affinity Gel. The active ATR kinase levels were determined by Western blotting of cellular lysates with a specific antibody against ATR and active forms of ATR (p-ATR Ser428).[45,46] UV-induced DNA damage can activate ATR by phosphorylating it at serine 428. The level of ATR was elevated in pcDNA3-ATR WT compared to the empty vector, though there was no major change in the ATR level in UV- treated and untreated samples (Figure S1). However, in UV-exposed conditions, the level of p-ATR was elevated compared to controls (Figure 2B). ATR (S428) is a marker of active ATR, indicating that the ATR protein purified after UV-C exposure was active ATR. Furthermore, ATR was eluted from the FLAG resin using 3× Flag peptide (Figure S2), and the level of p-ATR was checked using western blotting (Figure 2C). Previous studies have purified Flag-tagged ATR from hydroxyurea, and doxycycline-treated cells to achieve improved ATR kinase activity.[47,48] ADP-Glo assay was used to access the kinase activity of the purified ATR (Figure 2D), and

https://doi.org/10.1021/acsomega.2c07356
ACS Omega 2023, 8, 4954−4962

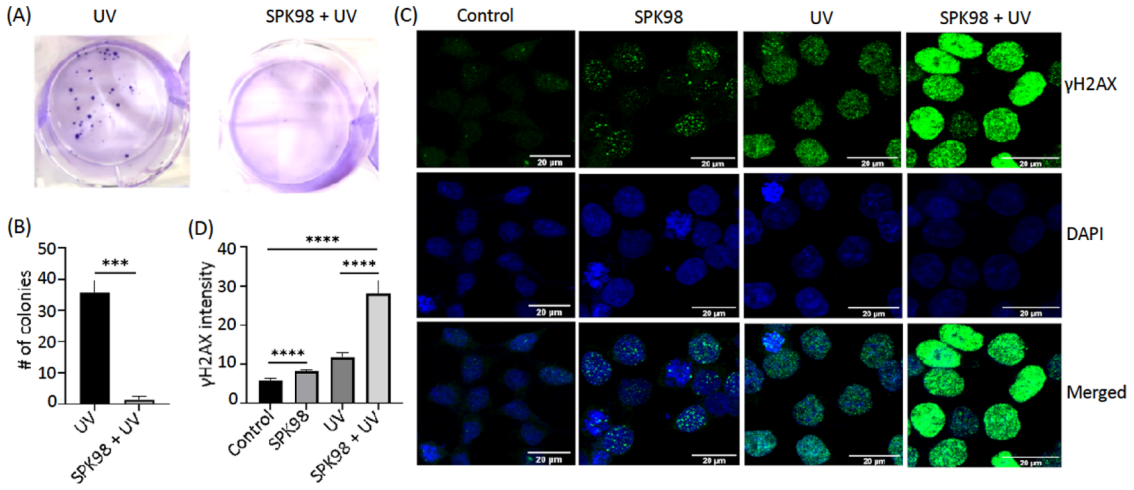

Figure 4. (A) Clonogenic assay of HCT116-ATM_KD cells in combinatorial treated with UV and SPK98. Representative images of single-cell clone proliferation, stained with crystal violet. (B) Quantification of the results, two-tailed unpaired Student *t*-test was performed using GraphPad Prism (***$P < 0.001$, $n = 3$). (C) Confocal microscopy image depicting a synergistic increase in γH2AX levels following UV+SPK98 treatment. DAPI was used to stain the cell nuclei. (D) Quantification of the γH2AX levels, two-tailed unpaired Student *t*-test was performed using GraphPad Prism (****$P < 0.0001$, $n = 3$).

we observed that purified, full-length ATR exhibits luminescence and is physiologically active (Figure 2E). The kinase activity was determined at the increasing amount of ATR protein (62−620 ng) and ATP (100−500 μM). A subsequent rise in the generation of ADP and, consequently, the kinase activity was observed as the protein amount and ATP concentration increased (Figure S3). In our assay, we used VX-970, a widely known ATR inhibitor alongside SPK98, to determine whether the inhibition of kinase reaction observed a similar luminescence signal. Based on the experimental findings and observations, we conclude that our purified ATR is moderately active, and the ATR inhibition potency of SPK98 is comparable to that of VX-970 (Figure 2E).

ATM or P53 Loss Confers Sensitivity to SPK98. With the notion that ATR inhibition in ATM- or P53-deficient cells leads to selective sensitization in cancer cells, we then explored the therapeutic potential of SPK98 in ATM- or P53-deficient cells. Toward this, ATM was knocked down in HCT116, and the expression of the ATM was checked using a western blot (Figure 3A). The level of ATM was observed to be significantly reduced in ATM knocked down (ATM_KD) cells. Following this, cell viability was performed in different cells with varying expression profiles of ATM or P53. The results showed that there is a significant difference in the GI_{50} value of SPK98 in ATM- or P53-deficient cells over proficient cells. The GI_{50} value of ATM_KD cells is more than 4 times lower than that of WT cells (Figure 3B,C). Similarly, cells lacking proficient P53 protein (MDAMD-231) exhibit an approximately 5-fold difference in GI_{50} valve compared to cells with proficient P53 protein (MCF7) (Figure 3D).

Furthermore, a clonogenic assay was performed to assess SPK98 potential to produce chromosomal anomalies due to compromised DNA repair or apoptosis, resulting in cell reproductive death. The clonogenic test was used to determine whether cells survived inhibitor treatments and preserved their capacity to proliferate post-treatment. The inhibition of cancer cells' unlimited growth ability is required to restrict tumor recurrence. SPK98-treated cells displayed a significant reduction in clonogenic potential compared to untreated cells (Figure 3E). Overall, this result implies that cells lacking the functional ATM/P53 pathway showed poor clonogenic potency at lower concentrations of SPK98 than WT cells.

SPK98 Is a Potent Radio-Sensitizing Agent. Clonogenic assay was used to evaluate the cellular radio-sensitivity of cancer cells in response to the combination of radiation therapy and SPK98 treatment. For this study, HCT116-ATM_KD cells were exposed to a relevant dose of UV-type C and SPK98. Following this, the cells were allowed to grow over a period of 3−4 weeks. The surviving fraction of proliferating cells produced cell colonies. Cell colonies are then fixed and stained with crystal violet to make them visible. The results revealed a significant decrease in the number of surviving cells capable of forming colonies in SPK98-treated cells exposed to UV compared to only UV treatment (Figure 4A,B). Furthermore, there were hardly any surviving cells suggesting the reproductive death of the cells that received combinatorial treatment.

In response to DNA damaging UV-C irradiation, H2AX is phosphorylated at serine 139 (γH2AX), which is mediated by PIKK family members like ATR kinase.[49] γH2AX is a common marker used to determine the frequency of DNA double-strand breaks. It plays a role in the initiation of DNA repair processes. Effective DNA repair after inducing DNA damage would lead to a drop in the level of γH2AX.[50] The DNA repair process would be impeded after the induction of DNA damage followed by the inhibition of DNA repair proteins like ATR, leading to an elevated level of γH2AX. As observed in Figure 4C,D, combinatorial treatment of UV-C and SPK98 resulted in a synergistic increase in the γH2AX levels compared to mono-treatment of UV-C or SPK98, suggesting a compromised DNA repair process. Overall, the result suggests that, in contrast to UV-C mono-treatment, the combinatorial treatment of SPK98 and UV-C dramatically decreased clonogenic potency, possibly due to impeded DNA repair.

SPK98 Induces Apoptosis. To determine if the cell death induced by SPK98 in HCT116-ATM_KD cells is via apoptosis, we first studied the morphology of the cells following SPK98 treatment. We examined the cell morphology of HCT116-ATM_KD cells stained with DAPI under the microscope after 24 h of SPK98 treatment. SPK98-treated cells

https://doi.org/10.1021/acsomega.2c07356
ACS Omega 2023, 8, 4954−4962

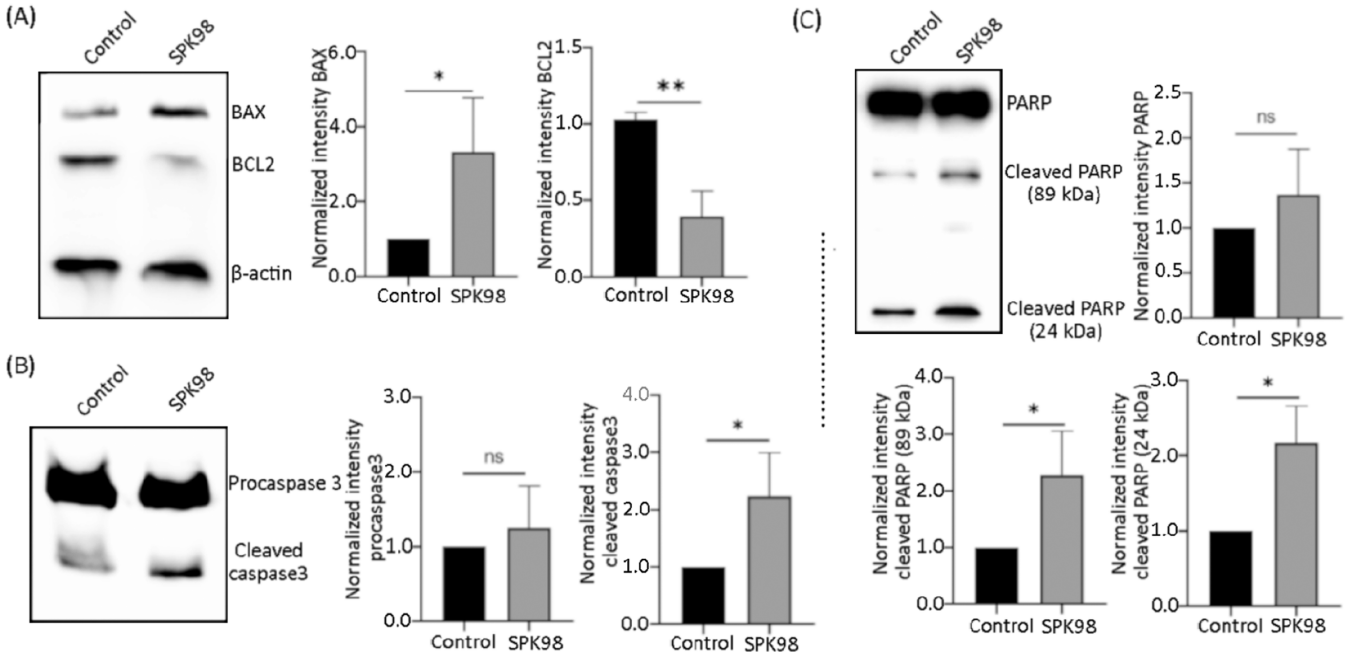

Figure 5. Western blot analyses of apoptosis markers in SPK98-treated and untreated HCT116-ATM_KD cells. (A) BCL2 and BAX levels and densitometry quantification, (B) procaspase-3 and cleaved caspase-3 levels along with densitometry quantification, (C) PARP and cleaved PARP levels along with densitometry quantification. Two-tailed unpaired Student *t*-test was performed using GraphPad Prism (*$P < 0.05$, **$P < 0.001$, $n = 3$).

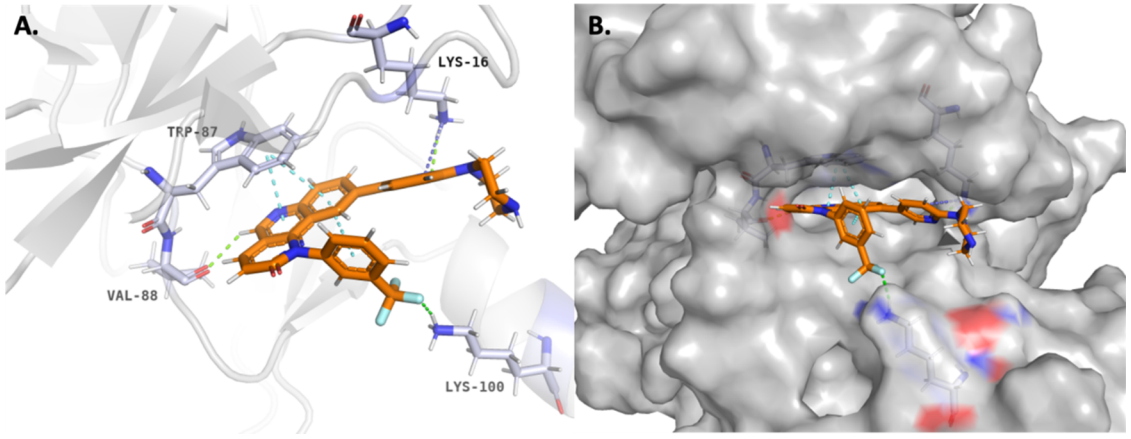

Figure 6. (A) Binding pose of SPK98 with ATR kinase modeled on PDB 4JSP. The orange color molecule is SPK98. Interacting residues are labeled appropriately. Green, light blue, and purple color dotted lines represent H-bonding interaction, $\pi\cdots\pi$ interactions, and cation$\cdots\pi$ interactions, respectively. (B) Surface representation of binding pocket and fitting of ligand in the cavity. Red and blue refer to the electronegative and electropositive zones of the binding cavity, respectively.

have fragmented nuclei, which is a characteristic of the late apoptotic stage,[51] as seen in Figure S4. To confirm this, we used western blot analysis using antibodies against apoptosis-related proteins to corroborate this finding. In SPK98-treated cells, the level of antiapoptotic protein BCL2 was reduced. On the other hand, the level of BAX, a pro-apoptotic protein whose oligomerization aids in the release of cytochrome C from mitochondria to the cytosol, was increased, which promotes apoptosis (Figure 5A). Similarly, the levels of cleaved caspase-3 were enhanced by a factor of 2 (Figure 5B). Caspases play a key role in controlling programmed cell death, and active caspase-3 is a commonly stimulated death protease that is responsible for degrading a variety of vital cellular proteins. There was also a substantial increase in the level of cleaved PARP protein. Caspases cleave PARP1 at its caspase-cleavage site, releasing 24 and 89 kDa fragments (Figure 5C). There was an overall rise in total PARP, which indirectly points to an upsurge in DNA strand breaks. PARP activation can result from DNA strand breaks, which could be the dying cell's attempt to repair the DNA damage. This PARP cleavage could prevent energy depletion, which is thought necessary for later stages of apoptosis. As a result, this cleaved form of PARP is often used as a marker of caspase-mediated apoptosis. All of these results point to the possibility that SPK98 induces apoptosis-mediated cell death.

Molecular Docking Analysis and Binding Energy Calculations. We performed an in silico analysis of SPK98's pharmacokinetic characteristics. A preliminary prediction of pharmacological properties can be helpful in identifying a molecule that can be effective as a drug and have the desired

https://doi.org/10.1021/acsomega.2c07356
ACS Omega 2023, 8, 4954−4962

biological effect while minimizing any unintended off-target effects. Some of the crucial ADME (absorption, distribution, metabolism, and excretion) characteristics of SPK98 are listed in Table S1. As can be seen from the table, the values for the chosen attributes were broadly within the acceptable range, suggesting that S9K98 may serve as a drug candidate, which warrants further in vivo studies.

Molecular docking analysis was performed on seven PIKK family proteins to better understand the interactions of SPK98 with these proteins. The rationale behind choosing these proteins is that torin2, the parent molecule of SPK98, is known to interact with them. Initially, molecular docking was performed in an extra precision mode to obtain the docking score and binding pose of SPK98 in the identified binding pockets of all of the selected proteins. The results summarized in Table S2 indicate that SPK98 has comparative docking scores on all of the selected proteins. To further quantify the interactions in terms of binding energy, MM-GBSA binding energies of the protein−ligand complexes were calculated. The MM-GBSA binding energy (ΔG_{bind}) is one of the accurate measures of the binding interaction between a protein and a ligand.[52] The ΔG_{bind} of protein−SPK98 complexes, as summarized in Table S2, show the order of strength of interactions. The binding energy calculated for the ATR−SPK98 complex is −58.80 kcal/mol. The ΔG_{bind} in the order ATM < ATR < PIK3C3 < PI4KB < mTOR < DNA-PK < PI3K-γ indicates the decreasing order of stability of the complexes. However, previously, we had not observed a significant ATM inhibition in cellular results.[38] In the case of ATM, SPK98 forms major interactions with Ala754 and Cys831 through H-bonding and $\pi\cdots\pi$ stacking with Trp830 (Figure S5A). On the other hand, the major contributing residues in the binding of SPK98 with ATR kinase are Trp87, which shows a characteristic $\pi\cdots\pi$ interaction, and Lys16, which shows H-bond and cation$\cdots\pi$ interaction with the pyridine ring. Val88 and Lys100 form weak C−H···O and N−H···F interactions with the ligand, respectively (Figure 6A). The hydrophobic amino acid residues in the binding pocket of mTOR, PIK3C3, and PI3K-γ are the major contributors to the docking scores (Figures S5B and S6). A significant volume is available to accommodate the SPK98 ligand placed parallelly to the hydrophobic amino acid residues. To corroborate the findings, we performed docking and ΔG_{bind} of Torin2 (Table S3, Supporting Information, SI), parent scaffold of SPK98, and a known mTOR inhibitor with off-target inhibition of other PIKK family proteins, including ATM and ATR at higher concentrations.[39] Wherein we again observed the best binding interaction energy of Torin2 with ATM followed by mTOR, though the docking score was highest with mTOR. This seems to be at odds with the enzyme and cell studies, where Torin2 is more selective against mTOR at a lower concentration.[39] A similar trend was observed for ATM in the case of SPK98 as well. We examined the ATM model structure to comprehend these opposing findings. The ATM model structure has a flexible loop region containing Gln935 residue, which forms an NH···F type of hydrogen-bonding interaction between Torin2 and Gln935. Torin2−ATM complex is stabilized by strong H-bond interaction, $\pi\cdots\pi$ stacking, and NH···F interactions (2.6 Å), which contributes to the smaller binding free energy of the complex, as shown in Figure S5C. However, in the case of mTOR and ATR, the flexible loop resides far away from the trifluoromethyl phenyl group, thereby lacking the additional interactions through Gln residue (Figure S5B,D). The overlay of the energy-minimized protein−ligand complexes of SPK98 with ATM, ATR, and mTOR shown in Figure S7 clearly show the presence of additional interactions occurring due to a more flexible loop of ATM compared to that in ATR and mTOR. The lower binding free energy in the Torin2−ATM and SPK98−ATM complexes due to additional interactions originating from an unresolved flexible loop may result in false positives. This could explain why in vitro results did not show a strong inhibition against ATM. Additionally, a well-resolved structure of these kinases would be helpful to fully comprehend the key dynamic influencing the binding of the molecules with these proteins.

CONCLUSIONS

The role of ATR and its implication in cancer has been well explored in the past few decades. However, only in the last 10 years have ATR inhibitors entered the clinical trial. The advancement in genomic screen techniques has facilitated the identification of genetic determinants for drug sensitivity. These markers can be put to an advantage for selective cancer cell sensitization by employing the concept of synthetic lethality. Currently, the ATR inhibitors in the clinical trial are employed for different cancer types with DDR aberrations like ATM and P53 mutations. With a primary focus on colorectal cancer, this study explores the selectivity of SPK98 in ATM/P53-deficient and mutant cells across different cancer types. The findings suggest a differential selectivity of SPK98 over ATM/P53-deficient or mutant cells over wild type. Combinatorial treatment of UV treatment and SPK98 significantly nullified the population of surviving cells in comparison to UV treatment cells, suggesting its potential as adjuvant therapy. Furthermore, in vitro kinase assay from the purified WT ATR showed enzyme inhibition comparable to VX-970. Docking studies also suggest the specificity of SPK98 towards ATR and mTOR over another member of PIKK family proteins. QikProp analysis also predicts a good ADME profile of SPK98. Overall, this study suggests the potential of SPK98 to be explored in preclinical settings.

ASSOCIATED CONTENT

Supporting Information

The Supporting Information is available free of charge at https://pubs.acs.org/doi/10.1021/acsomega.2c07356.

ATR expression, FLAG-ATR in the elution fraction, ATR enzyme activity, nuclear fragmentation, molecular docking of SPK98 and Torin2, molecular docking of SPK98 with PIKK kinases, protein−ligand complex, ADME prediction profile of SPK98, docking score and MM-GBSA binding energies of SPK98, and Torin2 (PDF)

Accession Codes

Q13535: ATR, Q13315: ATM, P04637: P53, P42574: Caspase-3, Q07812: BAX, P10415: Bcl-2,P09874: PARP1.

AUTHOR INFORMATION

Corresponding Author

Sivapriya Kirubakaran − *Discipline of Chemistry, Indian Institute of Technology Gandhinagar, Gandhinagar 382355 Gujarat, India;* orcid.org/0000-0002-7200-7602; Email: priyak@iitgn.ac.in

https://doi.org/10.1021/acsomega.2c07356
ACS Omega 2023, 8, 4954−4962

Authors

Bhanu Priya − *Discipline of Biological Engineering, Indian Institute of Technology Gandhinagar, Gandhinagar 382355 Gujarat, India*

Gurudutt Dubey − *Discipline of Chemistry, Indian Institute of Technology Gandhinagar, Gandhinagar 382355 Gujarat, India*

Complete contact information is available at: https://pubs.acs.org/10.1021/acsomega.2c07356

Author Contributions

B.P. and S.K. conceptualized and designed the study. B.P. performed and analyzed all of the cellular and enzyme studies. G.D. carried out molecular docking studies, and all authors did the analysis. B.P. wrote the manuscript. The manuscript was edited and proofread by all of the authors.

Funding

S.K. greatly acknowledges Kankuben Bakshirambhai Gelot Chair for the support. The authors thank DRDO for supporting G.D. fellowship.

Notes

The authors declare no competing financial interest.

■ ACKNOWLEDGMENTS

The authors are grateful to Rashmi Bhakuni and Althaf Shaik for the initial discussion on project conceptualization. They thank Srimadhavi Ravi for proofreading the article. They also thank the Indian Institute of Technology Gandhinagar for providing the infrastructure and facilities.

■ REFERENCES

(1) Jackson, S. P.; Bartek, J. The DNA-Damage Response in Human Biology and Disease. *Nature* **2009**, *461*, 1071−1078.

(2) Cooke, M. S.; Evans, M. D.; Dizdaroglu, M.; Lunec, J. Oxidative DNA Damage: Mechanisms, Mutation, and Disease. *FASEB J.* **2003**, *17*, 1195−1214.

(3) Cimprich, K. A.; Cortez, D. ATR: An Essential Regulator of Genome Integrity. *Nat. Rev. Mol. Cell Biol.* **2008**, *9*, 616−627.

(4) Shaltiel, I. A.; Krenning, L.; Bruinsma, W.; Medema, R. H. The Same, Only Different—DNA Damage Checkpoints and Their Reversal throughout the Cell Cycle. *J. Cell Sci.* **2015**, *128*, 607−620.

(5) Weber, A. M.; Ryan, A. J. ATM and ATR as Therapeutic Targets in Cancer. *Pharmacol. Ther.* **2015**, *149*, 124−138.

(6) Giglia-Mari, G.; Zotter, A.; Vermeulen, W. DNA Damage Response. *Cold Spring Harbor Perspect. Biol.* **2011**, *3*, 1−19.

(7) Zou, L.; Elledge, S. J. Sensing DNA Damage through ATRIP Recognition of RPA-SsDNA Complexes. *Science* **2003**, *300*, 1542−1548.

(8) Shiotani, B.; Zou, L. ATR Signaling at a Glance. *J. Cell Sci.* **2009**, *122*, 301−304.

(9) Mordes, D. A.; Glick, G. G.; Zhao, R.; Cortez, D. TopBP1 Activates ATR through ATRIP and a PIKK Regulatory Domain. *Genes Dev.* **2008**, *22*, 1478−1489.

(10) Cortez, D.; Guntuku, S.; Qin, J.; Elledge, S. J. ATR and ATRIP: Partners in Checkpoint Signaling. *Science* **2001**, *294*, 1713−1716.

(11) Liu, Q.; Guntuku, S.; Cui, X. S.; Matsuoka, S.; Cortez, D.; Tamai, K.; Luo, G.; Carattini-Rivera, S.; DeMayo, F.; Bradley, A.; Donehower, L. A.; Elledge, S. J. Chk1 Is an Essential Kinase That Is Regulated by Atr and Required for the G2/M DNA Damage Checkpoint. *Genes Dev.* **2000**, *14*, 1448−1459.

(12) Liu, Y. P.; Zheng, C. C.; Huang, Y. N.; He, M. L.; Xu, W. W.; Li, B. Molecular Mechanisms of Chemo- and Radiotherapy Resistance and the Potential Implications for Cancer Treatment. *MedComm* **2021**, *2*, 315−340.

(13) Min, A.; Im, S.-A.; Jang, H.; Kim, S.; Lee, M.; Kim, D. K.; Yang, Y.; Kim, H.-J.; Lee, K.-H.; Kim, J. W.; Kim, T.-Y.; Oh, D.-Y.; Brown, J.; Lau, A.; O'connor, M. J.; Bang, Y.-J. AZD6738, A Novel Oral Inhibitor of ATR, Induces Synthetic Lethality with ATM Deficiency in Gastric Cancer Cells. *Mol. Cancer Ther.* **2017**, *16*, 566−577.

(14) Burdak-Rothkamm, S.; Rothkamm, K. DNA Damage Repair Deficiency and Synthetic Lethality for Cancer Treatment. *Trends Mol. Med.* **2021**, *27*, 91−92.

(15) Lee, J. M.; Ledermann, J. A.; Kohn, E. C. PARP Inhibitors for BRCA1/2 Mutation-Associated and BRCA-like Malignancies. *Ann. Oncol.* **2014**, *25*, 32−40.

(16) Guo, G.; Zhang, F.; Gao, R.; Delsite, R.; Feng, Z.; Powell, S. N. DNA Repair and Synthetic Lethality. *Int. J. Oral Sci.* **2011**, *3*, 176−179.

(17) Del Vecchio, F.; Mastroiaco, V.; Di Marco, A.; Compagnoni, C.; Capece, D.; Zazzeroni, F.; Capalbo, C.; Alesse, E.; Tessitore, A. Next-Generation Sequencing: Recent Applications to the Analysis of Colorectal Cancer. *J. Transl. Med.* **2017**, *15*, 1−19.

(18) Schweiger, T.; Liebmann-Reindl, S.; Glueck, O.; Starlinger, P.; Laengle, J.; Birner, P.; Klepetko, W.; Pils, D.; Streubel, B.; Hoetzenecker, K. Mutational Profile of Colorectal Cancer Lung Metastases and Paired Primary Tumors by Targeted next Generation Sequencing: Implications on Clinical Outcome after Surgery. *J. Thorac. Dis.* **2018**, *10*, 6147−6157.

(19) Randon, G.; Fucà, G.; Rossini, D.; Raimondi, A.; Pagani, F.; Perrone, F.; Tamborini, E.; Busico, A.; Peverelli, G.; Morano, F.; Niger, M.; Antista, M.; Corallo, S.; Saggio, S.; Borelli, B.; Zucchelli, G.; Milione, M.; Pruneri, G.; Di Bartolomeo, M.; Falcone, A.; de Braud, F.; Cremolini, C.; Pietrantonio, F. Prognostic Impact of ATM Mutations in Patients with Metastatic Colorectal Cancer. *Sci. Rep.* **2019**, *9*, No. 2858.

(20) Oren, M.; Rotter, V. Mutant P53 Gain-of-Function in Cancer. *Cold Spring Harbor Perspect. Biol.* **2010**, *2*, No. a001107.

(21) Jiang, H.; Reinhardt, H. C.; Bartkova, J.; Tommiska, J.; Blomqvist, C.; Nevanlinna, H.; Bartek, J.; Yaffe, M. B.; Hemann, M. T. The Combined Status of ATM and P53 Link Tumor Development with Therapeutic Response. *Genes Dev.* **2009**, *23*, 1895−1909.

(22) Austen, B.; Skowronska, A.; Baker, C.; Powell, J. E.; Gardiner, A.; Oscier, D.; Majid, A.; Dyer, M.; Siebert, R.; Taylor, A. M.; Moss, P. A.; Stankovic, T. Mutation Status of the Residual ATM Allele Is an Important Determinant of the Cellular Response to Chemotherapy and Survival in Patients with Chronic Lymphocytic Leukemia Containing an 11q Deletion. *J. Clin. Oncol.* **2007**, *25*, 5448−5457.

(23) Rahko, E.; Blanco, G.; Soini, Y.; Bloigu, R.; Jukkola, A. A Mutant TP53 Gene Status Is Associated with a Poor Prognosis and Anthracycline-Resistance in Breast Cancer Patients. *Eur. J. Cancer* **2003**, *39*, 447−453.

(24) Bertheau, P.; Turpin, E.; Rickman, D. S.; Espié, M.; De Reyniès, A.; Feugeas, J. P.; Plassa, L. F.; Soliman, H.; Varna, M.; De Roquancourt, A.; Lehmann-Che, J.; Beuzard, Y.; Marty, M.; Misset, J. L.; Janin, A.; De Thę, H. Exquisite Sensitivity of TP53 Mutant and Basal Breast Cancers to a Dose-Dense Epirubicin-Cyclophosphamide Regimen. *PLoS Med.* **2007**, *4*, No. e90.

(25) Fearon, E. R.; Vogelstein, B. A Genetic Model for Colorectal Tumorigenesis. *Cell* **1990**, *61*, 759−767.

(26) Zaidi, S. H.; Harrison, T. A.; Phipps, A. I.; Steinfelder, R.; Trinh, Q. M.; Qu, C.; Banbury, B. L.; Georgeson, P.; Grasso, C. S.; Giannakis, M.; Adams, J. B.; Alwers, E.; Amitay, E. L.; Barfield, R. T.; Berndt, S. I.; Borozan, I.; Brenner, H.; Brezina, S.; Buchanan, D. D.; Cao, Y.; Chan, A. T.; Chang-Claude, J.; Connolly, C. M.; Drew, D. A.; Farris, A. B.; Figueiredo, J. C.; French, A. J.; Fuchs, C. S.; Garraway, L. A.; Gruber, S.; Guinter, M. A.; Hamilton, S. R.; Harlid, S.; Heisler, L. E.; Hidaka, A.; Hopper, J. L.; Huang, W. Y.; Huyghe, J. R.; Jenkins, M. A.; Krzyzanowski, P. M.; Lemire, M.; Lin, Y.; Luo, X.; Mardis, E. R.; McPherson, J. D.; Miller, J. K.; Moreno, V.; Mu, X. J.; Nishihara, R.; Papadopoulos, N.; Pasternack, D.; Quist, M. J.; Rafikova, A.; Reid, E.E.G.; Shinbrot, E.; Shirts, B. H.; Stein, L. D.; Teney, C. D.; Timms, L.; Um, C. Y.; Van Guelpen, B.; Van Tassel, M.; Wang, X.; Wheeler, D. A.; Yung, C. K.; Hsu, L.; Ogino, S.; Gsur, A.; Newcomb, P. A.;

Gallinger, S.; Hoffmeister, M.; Campbell, P. T.; Thibodeau, S. N.; Sun, W.; Hudson, T. J.; Peters, U. Landscape of Somatic Single Nucleotide Variants and Indels in Colorectal Cancer and Impact on Survival. *Nat. Commun.* **2020**, *11*, No. 3644.
(27) Reinhardt, H. C.; Aslanian, A. S.; Lees, J. A.; Yaffe, M. B. P53-Deficient Cells Rely on ATM- and ATR-Mediated Checkpoint Signaling through the P38MAPK/MK2 Pathway for Survival after DNA Damage. *Cancer Cell* **2007**, *11*, 175−189.
(28) Reaper, P. M.; Griffiths, M. R.; Long, J. M.; Charrier, J. D.; MacCormick, S.; Charlton, P. A.; Golec, J.M.C.; Pollard, J. R. Selective Killing of ATM- or P53-Deficient Cancer Cells through Inhibition of ATR. *Nat. Chem. Biol.* **2011**, *7*, 428−430.
(29) Sheng, H.; Huang, Y.; Xiao, Y.; Zhu, Z.; Shen, M.; Zhou, P.; Guo, Z.; Wang, J.; Wang, H.; Dai, W.; Zhang, W.; Sun, J.; Cao, C. ATR Inhibitor AZD6738 Enhances the Antitumor Activity of Radiotherapy and Immune Checkpoint Inhibitors by Potentiating the Tumor Immune Microenvironment in Hepatocellular Carcinoma. *J. Immunother. Cancer* **2020**, *8*, No. e000340.
(30) Kanoh, Y.; Tamai, K.; Shirahige, K. Different Requirements for the Association of ATR−ATRIP and 9-1-1 to the Stalled Replication Forks. *Gene* **2006**, *377*, 88−95.
(31) Yan, S.; Michael, W. M. Cell Cycle TopBP1 and DNA Polymerase Alpha-Mediated Recruitment of the 9-1-1 Complex to Stalled Replication Forks: Implications for a Replication Restart-Based Mechanism for ATR Checkpoint Activation. *Cell Cycle* **2009**, *8*, 2877−2884.
(32) Middleton, M. R.; Dean, E.; Evans, T.R.J.; Shapiro, G. I.; Pollard, J.; Hendriks, B. S.; Falk, M.; Diaz-Padilla, I.; Plummer, R. Phase 1 Study of the ATR Inhibitor Berzosertib (Formerly M6620, VX-970) Combined with Gemcitabine ± Cisplatin in Patients with Advanced Solid Tumours. *Br. J. Cancer* **2021**, *125*, 510−519.
(33) Zimmermann, A.; Dahmen, H.; Grombacher, T.; Pehl, U.; Blaukat, A.; Zenke, F. T. Abstract 2588: M1774, a Novel Potent and Selective ATR Inhibitor, Shows Antitumor Effects as Monotherapy and in Combination. *Cancer Res.* **2022**, *82*, 2588.
(34) Dillon, M. T.; Boylan, Z.; Smith, D.; Guevara, J.; Mohammed, K.; Peckitt, C.; Saunders, M.; Banerji, U.; Clack, G.; Smith, S. A.; Spicer, J. F.; Forster, M. D.; Harrington, K. J. PATRIOT: A Phase I Study to Assess the Tolerability, Safety and Biological Effects of a Specific Ataxia Telangiectasia and Rad3-Related (ATR) Inhibitor (AZD6738) as a Single Agent and in Combination with Palliative Radiation Therapy in Patients with Solid Tumours. *Clin. Transl. Radiat. Oncol.* **2018**, *12*, 16−20.
(35) Roulston, A.; Zimmermann, M.; Papp, R.; Skeldon, A.; Pellerin, C.; Dumas-Bérube, É.; Dumais, V.; Dorich, S.; Fader, L. D.; Fournier, S.; Li, L.; Leclaire, M. E.; Yin, S. Y.; Chefson, A.; Alam, H.; Yang, W.; Fugère-Desjardins, C.; Vignini-Hammond, S.; Skorey, K.; Mulani, A.; Rimkunas, V.; Veloso, A.; Hamel, M.; Stocco, R.; Mamane, Y.; Li, Z.; Young, J.T.F.; Zinda, M.; Black, W. C. RP-3500: A Novel, Potent, and Selective ATR Inhibitor That Is Effective in Preclinical Models as a Monotherapy and in Combination with PARP Inhibitors. *Mol. Cancer Ther.* **2022**, *21*, 245−256.
(36) Patel, M.; Moore, K. N.; Piscitello, D.; Majithiya, J.; Luzarraga, M. R.; Millward, H.; Holt, S. V.; Johnson, M. Abstract LB520: A Pharmacodynamic Platform Using Liquid Biopsy to Support Dose Selection for the ATR Inhibitor ART0380 (IACS-030380). *Cancer Res.* **2022**, *82*, LB520.
(37) Shaik, A.; Bhakuni, R.; Kirubakaran, S. Design, Synthesis, and Docking Studies of New Torin2 Analogs as Potential ATR/MTOR Kinase Inhibitors. *Molecules* **2018**, *23*, 992.
(38) Bhakuni, R.; Shaik, A.; Priya, B.; Kirubakaran, S. Characterization of SPK 98, a Torin2 Analog, as ATR and MTOR Dual Kinase Inhibitor. *Bioorg. Med. Chem. Lett.* **2020**, *30*, No. 127517.
(39) Liu, Q.; Xu, C.; Kirubakaran, S.; Zhang, X.; Hur, W.; Liu, Y.; Kwiatkowski, N. P.; Wang, J.; Westover, K. D.; Gao, P.; Ercan, D.; Niepel, M.; Thoreen, C. C.; Kang, S. A.; Patricelli, M. P.; Wang, Y.; Tupper, T.; Altabef, A.; Kawamura, H.; Held, K. D.; Chou, D. M.; Elledge, S. J.; Janne, P. A.; Wong, K. K.; Sabatini, D. M.; Gray, N. S. Characterization of Torin2, an ATP-Competitive Inhibitor of MTOR, ATM, and ATR. *Cancer Res.* **2013**, *73*, 2574−2586.
(40) Friesner, R. A.; Banks, J. L.; Murphy, R. B.; Halgren, T. A.; Klicic, J. J.; Mainz, D. T.; Repasky, M. P.; Knoll, E. H.; Shelley, M.; Perry, J. K.; Shaw, D. E.; Francis, P.; Shenkin, P. S. Glide: A New Approach for Rapid, Accurate Docking and Scoring. 1. Method and Assessment of Docking Accuracy. *J. Med. Chem.* **2004**, *47*, 1739−1749.
(41) Gohlke, H.; Klebe, G. Approaches to the description and prediction of the binding affinity of small-molecule ligands to macromolecular receptors. *Angew. Chem., Int. Ed.* **2002**, *41*, 2644−2676.
(42) Chen, Y.; Yuan, J. The Post Translational Modification of Key Regulators of ATR Signaling in DNA Replication. *Genome Instab. Dis.* **2021**, *2*, 92−101.
(43) Vrouwe, M. G.; Pines, A.; Overmeer, R. M.; Hanada, K.; Mullenders, L. H. F. UV-Induced Photolesions Elicit ATR-Kinase-Dependent Signaling in Non-Cycling Cells through Nucleotide Excision Repair-Dependent and -Independent Pathways. *J. Cell Sci.* **2011**, *124*, 435−446.
(44) Beyaert, M.; Starczewska, E.; Pérez, A.C.G.; Vanlangendonck, N.; Saussoy, P.; Tilman, G.; Leener, A.; De; Vekemans, M. C.; Van Den Neste, E.; Bontemps, F. Reevaluation of ATR Signaling in Primary Resting Chronic Lymphocytic Leukemia Cells: Evidence for pro-Survival or pro-Apoptotic Function. *Oncotarget* **2017**, *8*, 56906.
(45) Vauzour, D.; Vafeiadou, K.; Rice-Evans, C.; Cadenas, E.; Spencer, J. P. E. Inhibition of Cellular Proliferation by the Genistein Metabolite 5,7,3′,4′-Tetrahydroxyisoflavone Is Mediated by DNA Damage and Activation of the ATR Signalling Pathway. *Arch. Biochem. Biophys.* **2007**, *468*, 159−166.
(46) Feng, W.; Dean, D. C.; Hornicek, F. J.; Wang, J.; Jia, Y.; Duan, Z.; Shi, H. ATR and P-ATR Are Emerging Prognostic Biomarkers and DNA Damage Response Targets in Ovarian Cancer. *Ther. Adv. Med. Oncol.* **2020**, *12*, No. 1758835920982853.
(47) Cliby, W. A.; Roberts, C. J.; Cimprich, K. A.; Stringer, C. M.; Lamb, J. R.; Schreiber, S. L.; Friend, S. H. Overexpression of a Kinase-Inactive ATR Protein Causes Sensitivity to DNA-Damaging Agents and Defects in Cell Cycle Checkpoints. *EMBO J.* **1998**, *17*, 159−169.
(48) Liu, S.; Shiotani, B.; Lahiri, M.; Maré Chal, A.; Tse, A.; Chung, C.; Leung, Y.; Glover, J. N. M.; Yang, X. H.; Zou, L. Article ATR Autophosphorylation as a Molecular Switch for Checkpoint Activation. *Mol. Cell* **2011**, *43*, 192−202.
(49) Hanasoge, S.; Ljungman, M. H2AX Phosphorylation after UV Irradiation Is Triggered by DNA Repair Intermediates and Is Mediated by the ATR Kinase. *Carcinogenesis* **2007**, *28*, 2298−2304.
(50) Bonner, W. M.; Redon, C. E.; Dickey, J. S.; Nakamura, A. J.; Sedelnikova, O. A.; Solier, S.; Pommier, Y. GammaH2AX and Cancer. *Nat. Rev. Cancer* **2008**, *8*, 957−967.
(51) Collins, J. A.; Schandl, C. A.; Young, K. K.; Vesely, J.; Willingham, M. C. Major DNA Fragmentation Is a Late Event in Apoptosis. *J. Histochem. Cytochem.* **1997**, *45*, 923−934.
(52) Genheden, S.; Ryde, U. The MM/PBSA and MM/GBSA Methods to Estimate Ligand-Binding Affinities. *Expert Opin. Drug Discovery* **2015**, *10*, 449−461.

https://doi.org/10.1021/acsomega.2c07356
ACS Omega 2023, 8, 4954−4962